CFD SIMULATIONS AND WIND TUNNEL EXPERIMENTS FOR RE-USABLE LAUNCH VEHICLES

*Jan Vos, Dominique Charbonnier**

CFS Engineering
EPFL Innovation Park, Batiment A
1015 Lausanne, Switzerland

Ansgar Marwege, Christian Hantz, Ali Gülhan

DLR Institute of Aerodynamics and Flow Technology
Supersonic and Hypersonic Technologies Department
Linder Höhe, 51147 Cologne, Germany

ABSTRACT

In the frame of the RETALT project a large number of CFD simulations and Wind Tunnel experiments were made for both the RETALT1 and RETALT2 configurations to better understand the physics and mechanisms of retro-propulsion at supersonic flow conditions. For RETALT1, it was found in both CFD and Wind Tunnel experiments that the flow structure (bow shock stand-off distance, location of the Mach disk) varies linearly with $\sqrt{(c_T)}$, with c_T the thrust coefficient. However, other flow features, as for example the ratio of nozzle exit pressure with the post-stagnation pressure, show a linear dependence on the c_T. For RETALT2 a hysteresis effect was observed in the Wind Tunnel experiments when varying the incidence angle, and a similar behavior was found in the CFD calculations.

Index Terms— Reusable launchers, Computational Fluid Dynamics, Wind Tunnel Experiments

1. INTRODUCTION

In the frame of the EU funded Horizon2020 project RETALT (Retro Propulsion Assisted Landing Technologies) critical technologies for reusable launch vehicles are studied. Aerodynamics is one of these critical technologies, and a large number of Wind Tunnel experiments and CFD simulations were made for a Two Stage To Orbit (TSTO) Vertical Take-off Vertical Landing (VTVL) Launcher configuration similar to the Falcon 9 by SpaceX (RETALT1), and a small Single Stage To Orbit (SSTO) Launcher (RETALT2), see Fig. 1.
RETALT1 was designed to transport 20 tons to a Low Earth Orbit (LEO) or 14 tons to the Geostationary Transfer Orbit (GTO). RETALT1 uses for both the first and second stage an engine similar to the Vulcain 2 engine using liquid Oxygen and Hydrogen (LOX/LH2). The first stage is powered by 9 engines, and will be recovered using retro-propulsion either by returning to the launch side, or by landing on a sea-going platform. When entering the earth atmosphere the aerodynamic control surfaces are deployed, and at around 70 km altitude a braking maneuver is made using 3 active engines. This is followed by an aerodynamic phase with only the central engine active to decelerate the first stage until touchdown.
RETALT2 is much smaller than RETALT1, and was designed to bring a payload of 500 kg into LEO. RETALT2 is using 9 engines similar to the Vinci engine. When returing to earth the conical shape will provide the aerodynamic deceleration and no re-entry burn will be necessary. This will reduce the fuel consumption when making a Down Range Landing. RETALT2 should be more considered as a technology test bed because critical technologies are less mature compared to RETALT1.
For RETALT1 this paper is concerned with the interaction of the retro-propulsion using 3 active engines with the incoming flow when making the breaking maneuver. Results of both wind tunnel experiments and CFD simulations will be discussed. For RETALT2 this paper focuses on the rebuilding of wind tunnel experiments using CFD for varying angles of attack.

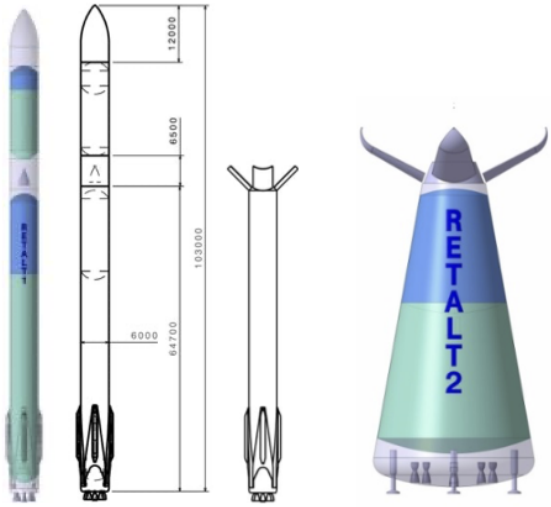

Fig. 1. RETALT1 TSTO (left) and RETALT2 (right) SSTO Configurations.

*Current address: Destinus, Aeropole 132, 1530 Payerne, Switzerland

2. DLR H2K WIND TUNNEL FACILITIES

A large series of Wind Tunnel tests were made in the different wind tunnel facilities at DLR in Cologne, see for more details [1].

2.1. Hypersonic Wind Tunnel Cologne(H2K)

The Hypersonic Wind Tunnel H2K is a blow down facility using pressurized air that permits to obtain Mach numbers between 4.8 and 11.2. The RETALT1 configuration has a scaling of a factor $1/130$ with respect to the flight configuration. In the wind tunnel experiments the plume was simulated using air that was blown through the model support sting.
Figure 2 shows an image of the RETALT1 configuration in the H2K facility. Measured data consisted of pressures at various locations in the base region and along the model, and Schlieren pictures. A comparison of measured and computed pressures can be found in [2].

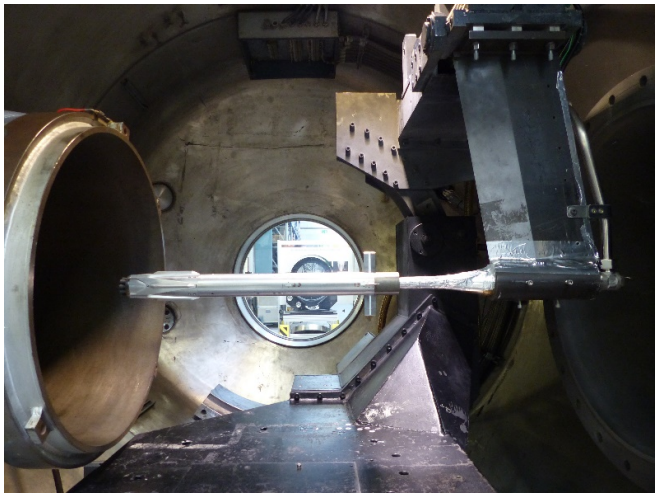

Fig. 2. The RETALT1 model in the H2K facility.

2.2. Trisonic Wind Tunnel Cologne(TMK)

The Trisonic Wind Tunnel Cologne (TMK) is a blow down wind tunnel with a Mach number range between 0.5 and 5.7, having a test section of $0.6 \times 0.6\ m$. The model adapter is compatible with the model adapter of the H2K, and it is possible to use the same model in both wind tunnels. Measured data for the RETALT2 configuration consisted of the aerodynamic forces, measured using a 6 components strain gauge balance, see also Fig. 3.

3. NSMB CFD SOLVER

The CFD calculations were made using the Navier Stokes Multi Block solver NSMB which is developed in a consortium composed of different universities and industries [3].

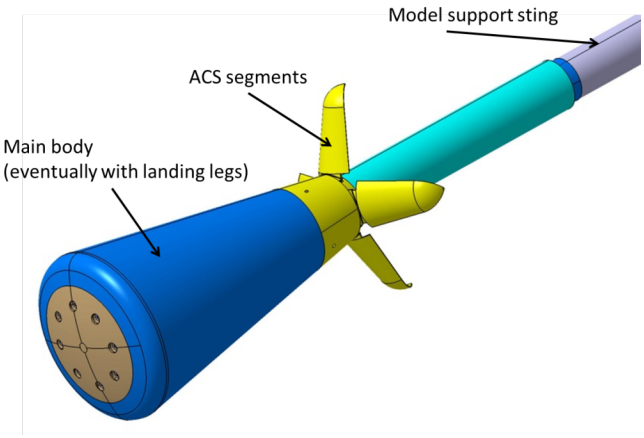

Fig. 3. RETALT2 Wind Tunnel model.

NSMB is a cell-centered finite volume solver using multi block structured grids. The patch grid and chimera method are available to simplify the mesh generation for complex geometries. Different turbulence models are available, among them the one-equation Spalart-Allmaras turbulence model [4] used in the simulations discussed in this paper.
NSMB includes a large variety of chemistry models for hypersonic applications. The chemistry modeling for the simulations at flight conditions including retro-propulsion is based on the thermally perfect gas assumption, with a mixture of 9 species (Nasa9 polynomial species). Mass fraction of species in the main flow (N2, O2) and in the exhaust gas (H2O, OH, H2, O2, ...) are applied as boundary conditions for computations with one or three engines active. The engine conditions are applied at the throat of the nozzles of the active engines.
Ansys ICEMCFD was used to generate the grids for the RETALT1 and RETALT2 configurations. The patched mesh approach as well as the Chimera overlapping grid technique were used to simplify the mesh generation. O-grid topologies with a geometric cell distribution were employed close to the solid walls to resolve the boundary layer. The first cell height in the wall normal direction was set to obtain an y^+ value below 1 required for the low turbulence model approach used. The growth ratio of the cells normal to the wall was set close to 1.2. The mesh in the bow shock region was refined to better improve the capturing of the bow shock wave. Figure 4 shows a picture of the grid for RETALT1 (showing only every 2nd grid point). The grid used for the Wind tunnel simulations had about 20 Million cells; for the flight simulations 2 configurations were used, one including the control surfaces (21 Million cells), and one using only the forebody of the launcher (12 Million cells). The grids were made such that it was possible to activate the different engines by simply changing a boundary condition.
For RETALT2 the focus was on the configuration with 45^o deflected control surfaces. This grid had around 13.6 Million cells.

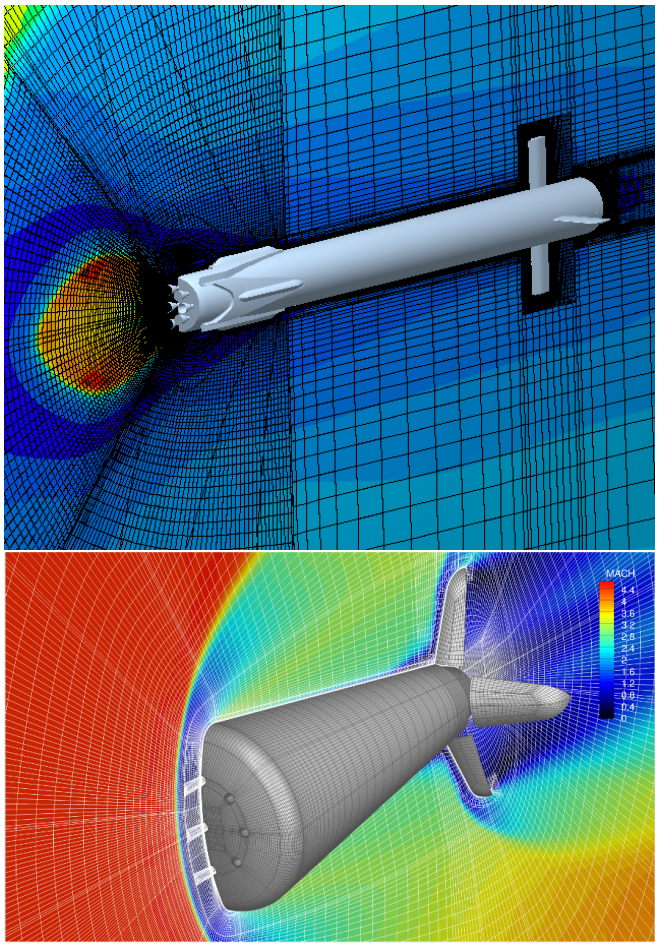

Fig. 4. View of the CFD grid in the symmetry plane for the RETALT1 (top) and RETALT2 (bottom) configurations.

4. RETALT1 CONFIGURATION

4.1. Simulation conditions

Table 1 summarizes the simulation conditions, with ϵ the nozzle expansion ratio. Missing in this table is the nozzle total pressure, which depends on the gas injected in the plume. For the simulations rebuilding the wind tunnel experiments air was used with total pressures varying between 4.6 and 25 bars (but it should be mentioned that in the wind tunnel experiments with 3 active engines the total pressure was limited to 12 bars). For the flight simulations total pressures were varied between 20 and 120 bars and depended on the gas injected in the plume (Air, LOX/LH2, LCH4/LO2, Helium). All calculations were made using 3 active engines.

The CFD simulations were made using the central space discretization scheme with artificial dissipation, and employing the LU-SGS semi-implicit scheme for the integration in time. Convergence was judged by looking at the convergence of the density L2-residue and of the drag coefficient. Calculations were made using the caloric perfect gas assumption (CPG) (when air was injected in the plume) or the thermal perfect gas (TPG) assumption. When using the thermal perfect gas assumption the thermodynamic properties of the gas mixture were calculated using the NASA data base using 9 polynomial coefficients [5]. Transport properties were in these simulations calculated using the Chemkin method [6].

Table 1. Simulation conditions

	Flight	Wind tunnel	
Mach number	5.3	5.29	$[-]$
Pressure	203.3	542.48	Pa
Temperature	257.54	68.21	K
Reynolds	$1.7\ 10^6$	$2.4\ 10^5$	$[-]$
T_t nozzle	3718.44	299.93	K
Nozzle expansion ratio ϵ	15.0	2.5	$[-]$

4.2. Retropropulsion

Retropropulsion is the situation when rocket engines are fired against the free-stream flow in order to decelerate the vehicle. For supersonic flows this leads to complex flow phenomena due to the interaction of the free-stream supersonic flow with the supersonic jet flow coming out of the nozzle [7], as illustrated in Fig. 5. In this picture one can clearly see the bow shock wave upstream of the configuration, the free stagnation surface where the incoming flow and the jet flow match, as well as the location of the Mach disk.

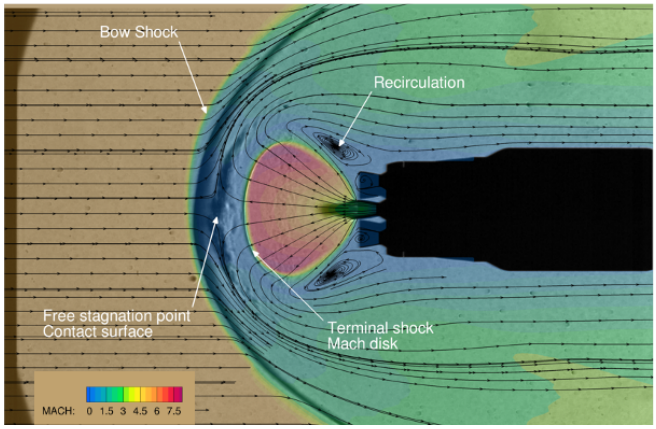

Fig. 5. The RETALT1 model in the H2K facility, computed Mach number contours with superimposed Schlieren picture.

The interaction between the free-stream flow and jet flow is characterized by the thrust coefficient c_T:

$$c_T = \frac{1}{M_\infty^2} \frac{p_e}{p_\infty} \frac{2A_e(1+\gamma_e M_\infty^2)}{\gamma_\infty A} \qquad (1)$$

where the subscript e indicates nozzle exit conditions, and

γ_e is the ratio of specific heats at the nozzle exit. The subscript ∞ indicates the free-stream conditions. The parameter A is the cross-sectional area of the rocket. As written in Eq. 1 the thrust coefficient can be written as a product of 3 terms, the first term showing the dependency on the free-stream Mach number, the second term, $\frac{p_e}{p_\infty}$ is the so called ambient pressure ratio (APR), and the last term the engine scaling parameter (ESP):

$$ESP = \frac{\gamma_\infty A}{2A_e(1+\gamma_e M_e^2)} \tag{2}$$

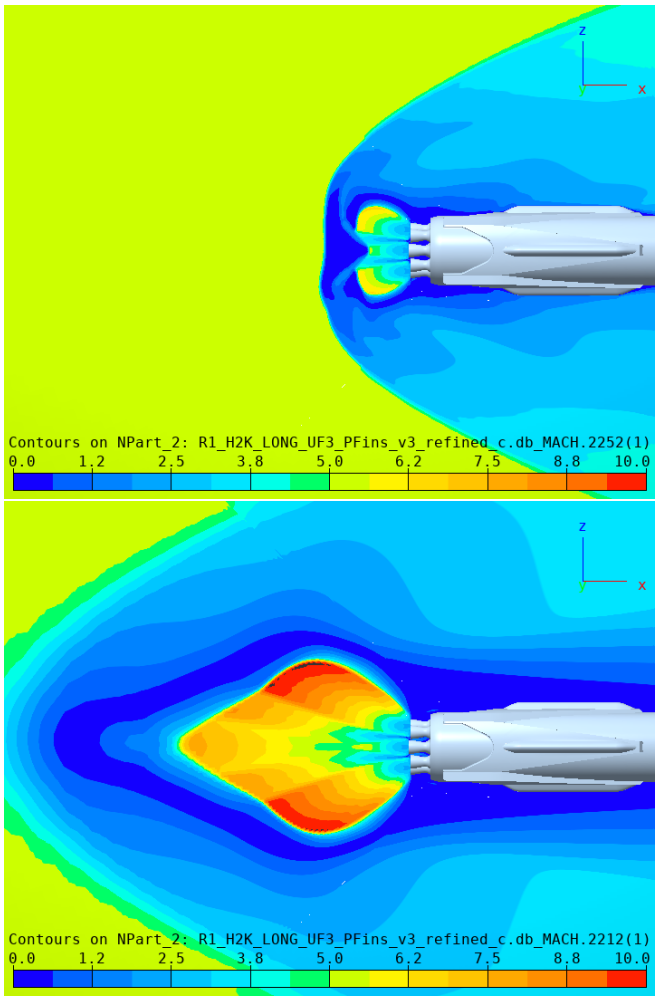

Fig. 6. Flow topologies for 3 active engines, very low c_T (top) and high c_T (bottom), H2K Wind tunnel model and H2K Wind Tunnel conditions.

For single engine nozzle flows, two types of flow topologies can be found [8]: the so-called jet penetration mode and the blunt mode, where the jet penetration mode occurs at low thrust coefficients, and the flow is in general unsteady. At higher trust coefficients the flow tends towards the blunt penetration mode. In our simulations using 3 engines, a blunt penetration mode was also observed at very low thrust coefficients, see Fig. 6.

The nozzle characteristics also influence the behavior of the nozzle exit flow. Calculations were made for the flight configuration scaled to the wind tunnel model size, using the H2K Wind Tunnel conditions summarized in Table 1. Figure 7 shows the flow topology of the scaled Flight configuration model for the same nozzle total pressure as the bottomm picture in Fig. 6. One clearly see large differences in flow topology, due to the larger nozzle expansion ratio of the (scaled) flight configuration. It was also observed that increasing the total pressure in the nozzle led for the H2K configuration earlier to an unsteady flow than for the scaled flight configuration.

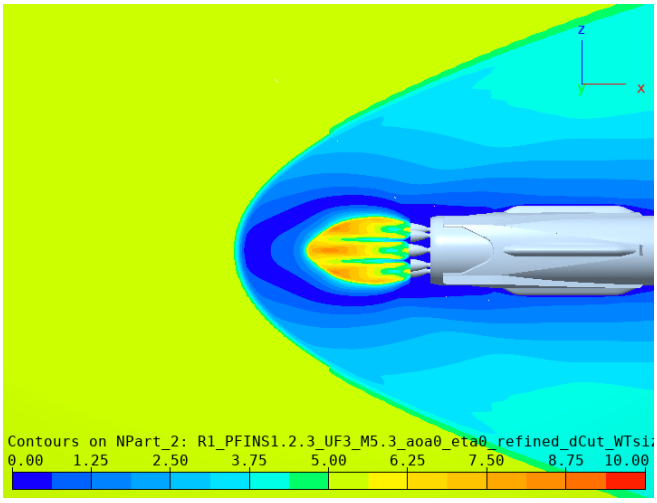

Fig. 7. Blunt mode flow topology for the scaled flight configuration, H2K Wind Tunnel conditions.

4.3. CFD simulations for different gas mixtures

A large number of CFD simulations were made for the flight configuration using different gas mixtures (H2-O2, CH4-O2, Air-TPG, Air-CPG, CH4, CO2, H2-HE, HE) for different total pressures in the nozzle. From the nozzle exit results the thrust coefficient Eq. (1) was computed, and for each calculation the locations of the bow shock, contact surface and terminal shock were extracted. The same was done for the calculations using the H2K model as well as of the scaled flight configuration computed for the H2K conditions. Figure 8 shows the normalized computed bow-shock stand-off distance versus the square root of the computed c_T using the nozzle exit conditions. As mentioned and shown in [7] a linear relationship was to be expected, and this was also found in the different simulations. The slope of these linear relationships depend strongly on the gas composition leaving the nozzle exit. One can observe that the slopes of the calculations for a caloric perfect gas (Air CPG, H2K UF3 and UF3-

WT) are close. If we look at the ratio of the specific heats γ_e at the nozzle exit one can observe that the slope increases as function of γ_e, see Fig. 8.

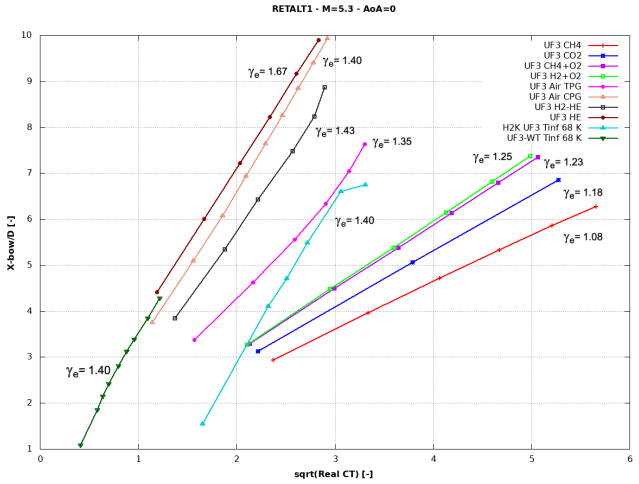

Fig. 8. Normalized bow shock stand-off distance versus $\sqrt{c_T}$ for different nozzle gases, flight and H2K configuration.

Another interesting parameter to study is the ratio of the nozzle exit pressure and the free-stream post-shock stagnation pressure $p_{0,2}$ that can be calculated from the normal shock relations, [7]:

$$\frac{p_e}{p_{0,2}} = \frac{p_e}{p_{t,\infty}} \left(\frac{(\gamma_\infty - 1)M_\infty^2 + 2}{(\gamma_\infty + 1)M_\infty^2}\right)^{\frac{\gamma_\infty}{\gamma_\infty - 1}} \left(\frac{2\gamma_\infty M_\infty^2 - (\gamma_\infty - 1)}{\gamma_\infty + 1}\right)^{\frac{1}{\gamma_\infty - 1}} \tag{3}$$

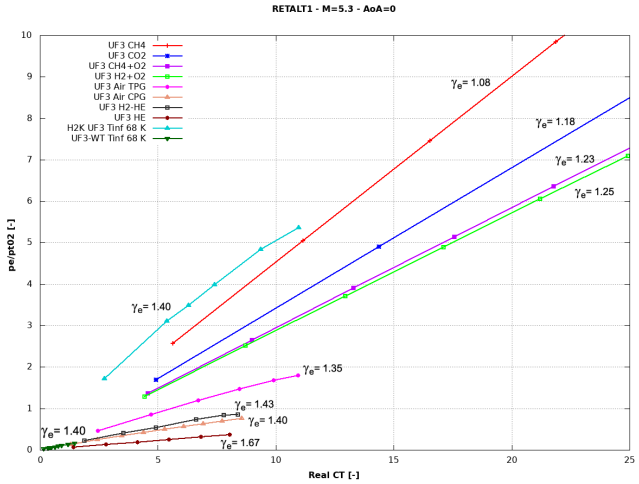

Fig. 9. Ratio nozzle exit pressure and free-stream post-shock stagnation pressure as function of c_T for different nozzle gases, flight and H2K configuration.

Figure 9 shows this relation as function of the computed trust coefficient, and as expected (because the Mach number is the same for all cases) one can observe a linear relationship which depends not only on the ratio of specific heats (the gas injected in the nozzle), but also on the nozzle expansion ratio as shown by the results of the H2K curve.

Figure 10 shows a comparison of the flow structures of the flight configuration (computed with the flight conditions using a caloric perfect gas air as jet), and of the scaled flight model (computed using the wind tunnel conditions). The nozzle expansion ratio in both calculations is the same, and the computed c_T for the calculations are close. This was obtained with a nozzle pressure of 20 $bars$ for the flight model and 50 $bars$ for the scaled model. Although the positions of the bow shock and terminal shock wave are not the same (a little farther away from the body for the scaled model), the flow structures and Mach numbers in the flow are comparable.

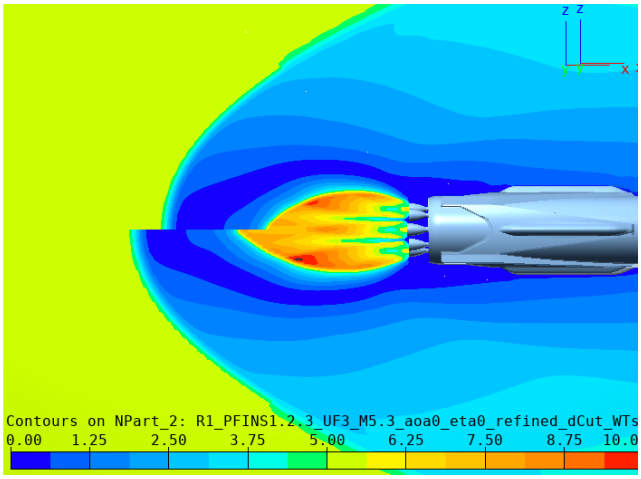

Fig. 10. Comparison of flow structure for the flight configuration (top) and the for same configuration scaled to the wind tunnel model size (bottom), c_T = 1.48.

Another interesting parameter to study is the Engine Scaling parameter ESP (Eq. 2). Figure 11 shows this parameter for the flight and wind tunnel conditions, for various gas mixtures in the nozzle. The figure also shows the value of the ratio of specific heats at the nozzle exit, γ_e. Except for the H2K conditions, one can observe that the ESP depends only on the value of γ_e. Further analysis of the results for the H2K conditions showed that the temperature at the nozzle exit decreased with increasing thrust coefficient. This was also observed for the other gas mixtures, but because the temperature at the nozzle exit is low for the H2K conditions, the influence of this temperature decrease (which directly affects the exit Mach number M_e through the speed of sound) is much larger compared to the simulations at flight conditions for the different gases used in the nozzle.

Figure 12 shows the plume structure for different gas mix-

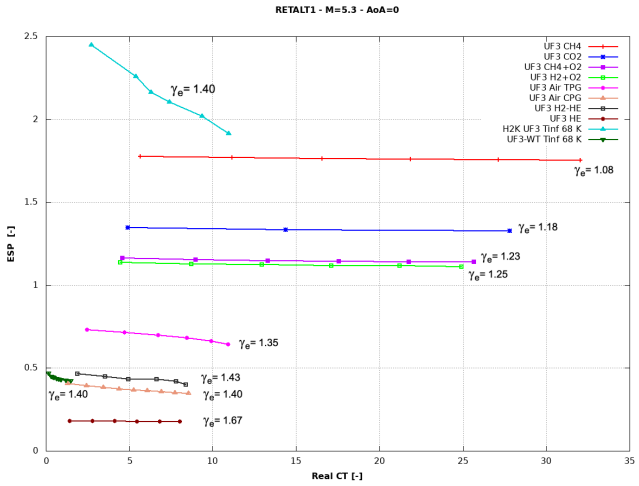

Fig. 11. Engine scaling parameter ESP (Eq. 2) versus the computed c_T for different gas mixtures.

tures, for the highest thrust coefficient. One can clearly observe the evolution of the shape of the plume as function of the ratio of the specific heats at the nozzle exit.

5. RETALT2 CONFIGURATION

5.1. Free stream conditions

Wind tunnel experiments were made in the TMK at Mach=1.5, and the conditions are summarized in Table 2. Different deflections of the aerodynamic control surfaces were used, [1], the paper here is concerned with the deflection of all control surfaces at 45^o.

Table 2. Simulation conditions

Mach number	1.5	$[-]$
Pressure	756.13	Pa
Temperature	231.25	K
Reynolds	4.56e5	$[1/m]$

5.2. CFD simulations

CFD simulations were made using the NSMB CFD solver to study the influence of the turbulence model, and to study the influence of the hysteresis effects found in the experiments. All CFD simulations were made using the central space discretization scheme, and the LU-SGS scheme for the integration in time. The calculations were made using both the Spalart-Allmaras 1-equation turbulence model [4] as well as the $k-\omega$ Menter Shear Stress (MSS) model [9]. For both turbulence models two sweeps were computed, the first one from $\alpha = 0^0$ to $\alpha = 10^0$ with an increment of 1^o, and the

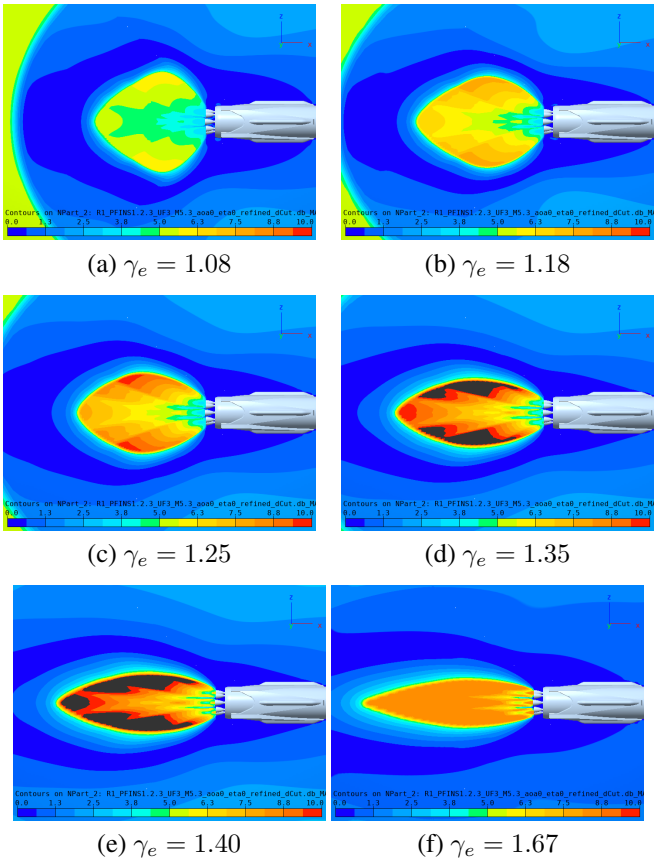

(a) $\gamma_e = 1.08$ (b) $\gamma_e = 1.18$

(c) $\gamma_e = 1.25$ (d) $\gamma_e = 1.35$

(e) $\gamma_e = 1.40$ (f) $\gamma_e = 1.67$

Fig. 12. Mach number contours to show the plume structure of the RETALT1 configuration as function of the gas mixture composition in the nozzle for the largest thrust coefficient, Mach=5.3, $\alpha = 0^o$

second one the opposite way. In both sweeps a first solution was computed at the first incidence angle (either 0^o or 10^o, and this solution was then used as starting solution for the next incidence angle.

Figure 14 shows the computed Mach number in the symmetry plane for an angle of attack of 10^o. The results in Figs. 14a and 14b were obtained by incrementing the incidence angle, while the results shown in Figs. 14c and 14d were obtained from the free-stream conditions. Several observations can be made:

- the flow separation starting at the shoulder computed using the $k-\omega$ turbulence model is larger compared to the flow separation obtained using the Spalart-Allmaras turbulence model.
- the flow structure in the base region is different for the two turbulence models
- for the Spalart-Allmaras turbulence model hysteresis effects are clearly visible in particular on the shoulder where the flow separation starts

- hysteresis effects are less pronounced when using the $k-\omega$ turbulence model

Figure 13 shows the measured and computed pitching and normal force coefficients. The hysteresis effects are clearly visible in the experiments. The CFD simulation show also hysteresis effects in the coefficients, more pronounced for the calculations using the $k-\omega$ turbulence model for angles of attacks between 3^o and 7^o. In general the results obtained with the Spalart-Allmaras turbulence model are in better agreement with the experimental results when the flow is attached and when the separation occors at about an angle of attack of 10^o, but the magnitude of the moment and forces for the separated flow is better predicted using the $k-\omega$ turbulence model.

6. CONCLUSIONS

Wind Tunnel experiments and CFD simulations were made for the RETALT1 and RETALT2 configurations. The focus of the studies for RETALT1 was the study of the interaction of the retro-propulsion with the incoming flow. Different gas mixtures were used, showing that the flow structure varies linearly with the square root of the thrust coefficient. This linear relationship depends on the gas mixture used in the nozzle.
For RETALT2 Wind Tunnel experiments showed hysteresis effects. These effects were also found in the CFD simulations using the Spalart-Allmaras and $k-\omega$ Menter Shear Stress turbulence models.

7. ACKNOWLEDGEMENTS

The RETALT project has received funding from the European Union's Horizon 2020 research and innovation framework program under Grant agreement No 821890.

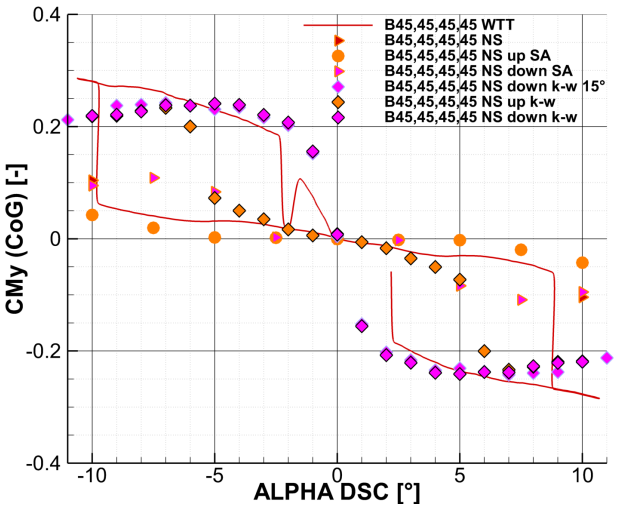

(a) CM_y

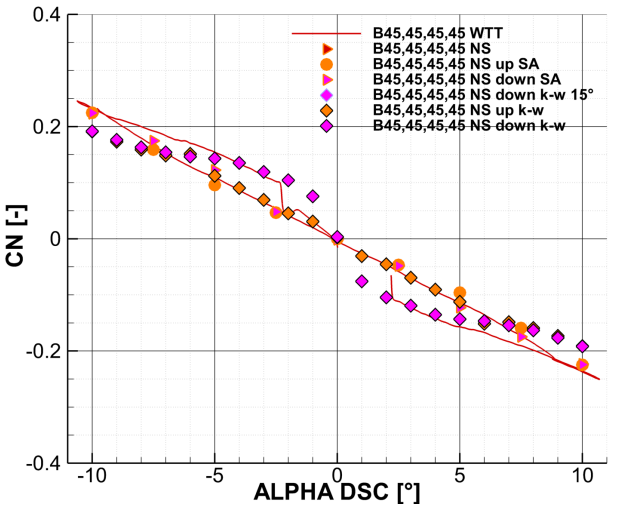

(b) CN

Fig. 13. Pitching moment coefficient and normal force coefficient as function of the incidence angle, RETALT2, Mach=1.5.

8. REFERENCES

[1] A. Marwege, C. Hantz, J. Vos, M. Laureti, S. Karl, D. Kirchheck, J. Klevanski, and A. Gülhan, *Aerodynamic Phenomena of Retro Propulsion Descent and Landing Configurations*, 2022.

[2] Jan B. Vos, Dominique Charbonnier, Ansgar Marwege, Ali Guelhan, Mariasole Laureti, and Sebastian Karl, *Aerodynamic investigations of a Vertical Landing Launcher configuration by means of Computational Fluid Dynamics and Wind Tunnel Tests*, AIAA Paper 6.2022-1308, 2022.

[3] Yannick Hoarau, Dorian Pena, Jan B. Vos, Dominique Charbonier, Alain Gehri, Marianna Braza, Thibaut Deloze, and Eric Laurendeau, *Recent Developments of the Navier Stokes Multi Block (NSMB) CFD solver*, AIAA Paper 6.2016-2056, 2016.

[4] P. Spalart and S. Allmaras, *A one-equation turbulence model for aerodynamic flows*, AIAA Paper 6.1992-439, 1992.

[5] B.J McBride and S. Gordon, "Computer program for calculation of complex chemical equilibrium compositions and applications ii users manual and program description," *NASA RP-1311-2*, 1996.

[6] R.J. Kee, F.M. Rupley, J.A. Miller, M.E. Coltrin, J.F. Grcar, E. Meeks, H.K. Moffat, A.E. Lutz, G. Dixon-Lewis, M.D. Smooke, J. Warnatz, G.H. Evans an R.S. Larson, R.E. Mitchell, L.R. Petzold, W.C. Reynolds, M. Caracotsios, W.E. Stewart, P. Glarborg, C. Wang, and O. Adi-

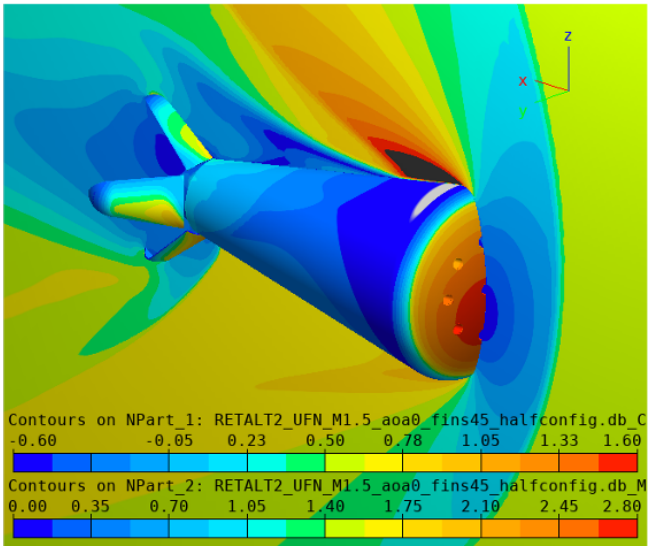

(a) Spalart-Allmaras model, $\alpha = 0 \rightarrow 10^o$

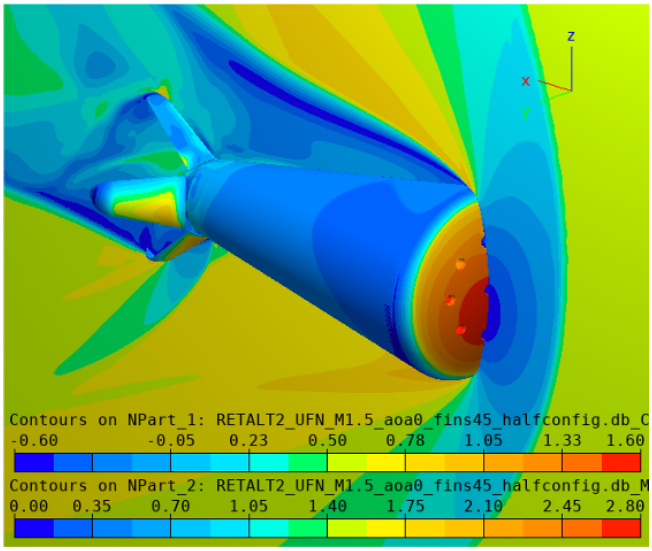

(b) k-ω MSS model, $\alpha = 0 \rightarrow 10^o$

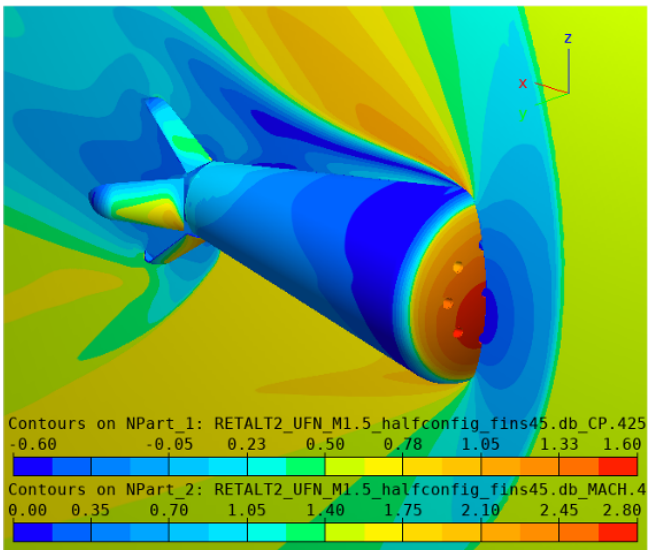

(c) Spalart-ALlmaras model, $\alpha = 10^o$

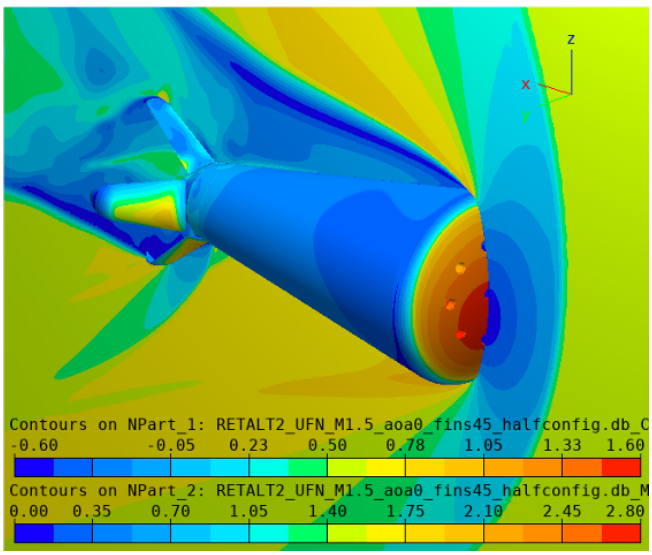

(d) k-ω MSS model, $\alpha = 10^o$

Fig. 14. RETALT2 configuration, Mach=1.5, $\alpha = 10^o$

gun, "Chemkin collection, release 3.6," *Reaction Design*, 2000.

[7] Kevin Gutsche, Ansgar Marwege, and Ali Gülhan, "Similarity and key parameters of retropropulsion assisted deceleration in hypersonic wind tunnels," *Journal of Spacecraft and Rockets*, vol. 58, no. 4, pp. 984–996, 2021.

[8] P.O. Jarvinen and R.H. Adams, "The aerodynamic characteristics of large angled cones with retrorockets," *NASA CR-124720*, 1970.

[9] F. Menter, *Zonal Two Equation k-w Turbulence Models For Aerodynamic Flows*, AIAA Paper 6.1993-2906, 1993.